IRIS AperTO

UNIVERSITÀ DEGLI STUDI DI TORINO

AperTO - Archivio Istituzionale Open Access dell'Università di Torino

Multicomponent T2 relaxometry reveals early myelin white matter changes induced by proton radiation treatment

This is the author's manuscript

Original Citation:

Availability:

This version is available http://hdl.handle.net/2318/1834210 since 2022-02-17T10:31:00Z

Published version:

DOI:10.1002/mrm.28913

Terms of use:

Open Access

Anyone can freely access the full text of works made available as "Open Access". Works made available under a Creative Commons license can be used according to the terms and conditions of said license. Use of all other works requires consent of the right holder (author or publisher) if not exempted from copyright protection by the applicable law.

(Article begins on next page)

16 October 2026

TECHNICAL NOTE

Multicomponent T_2 relaxometry reveals early myelin white matter changes induced by proton radiation treatment

Funding information Grant Fondazione CARITRO—via Calepina 1, 38122 Trento, Italy

AQ5 Pietro Bontempi [1,*] | Daniele Scartoni [1] | Dante Amelio [1] | Marco Cianchetti [1] | Ana Turkaj [1] | Maurizio Amichetti [1] | Paolo Farace [1]

AQ6 [1] Proton Therapy Unit, Hospital of Trento|Azienda Provinciale per i Servizi Sanitari (APSS), Trento, Italy

Correspondence

Pietro Bontempi, Proton Therapy Unit – Hospital of Trento, Azienda Provinciale per i Servizi Sanitari AQ3 (APSS), Via del Desert, 14 – 38122, Trento, Italy.

Email: pietro.bontempi@univr.it

Funding Information

Fondazione Cassa Di Risparmio Di Trento E Rovereto : 2018.0278

Abstract

Purpose

To investigate MRI myelin water imaging (MWI) by multicomponent T_2 relaxometry as a quantitative imaging biomarker for brain radiation-induced changes and to compare it with DTI.

Methods

Sixteen patients underwent fractionated proton therapy (PT) and received dose to the healthy tissue because of direct or indirect (base skull tumors) irradiation. MWI was performed by a multi-echo sequence with 32 equally spaced echoes (10-320 ms). Decay data were processed to identify 3 T_2 compartments: myelin water (Mw) below 40 ms, intra-extracellular water (IEw) between 40 and 250 ms, and free water (CSFw) above 250 ms. Both MWI and DTI scans were acquired pre (*pre*)-treatment and immediately at the end (*end*) of PT. After image registration, voxel-wise difference maps, obtained by subtracting MWI and DTI *pre* from those acquired at the *end* of PT, were compared with the corresponding biological equivalent dose (BED).

Results

Mw difference showed a positive correlation and IEw difference showed a negative correlation with BED considering *end–pre* changes ($P < .01$). The changes in CSFw were not significantly correlated with the delivered BED. The changes in DTI data, considering *end–pre* acquisitions, showed a positive correlation between fractional anisotropy and the delivered BED.

Conclusion

MWI might detect early white matter radiation-induced alterations, providing additional information to DTI, which might improve the understanding of the pathogenesis of the radiation damage.

Keywords

diffusion tensor imaging | DTI | multicomponent | MWI | myelin water imaging | proton therapy | radiotherapy | relaxation | T2

1 | INTRODUCTION

Radiation injury and complications of radiotherapy and chemotherapy on the central nervous system (CNS) have been investigated for many years,[1–4] but the large-scale neuro-mechanism and the post-radiation sequelae have not yet fully understood. It is realistic to assume that multiple cell targets (glial, neuronal, and endothelial blood vessel cells) are involved in radiation response.[5] Because radiation-induced white matter injury is associated with damage to oligodendrocytes,[5] myelin integrity can be compromised by the radiation insult. Transient demyelination is believed to be the underlying mechanism of early delayed reactions and the corresponding syndrome characterized by somnolence, which typically lasts for a few months after irradiation, followed by complete clinical recovery.[6] Demyelination and axonal degeneration/gliosis can be associated with late radiation-induced cognitive decline.[7] Demyelination was also described in the patients with the most severe late radiation-induced injury.[8]

Nowadays, several MRI methods are available for the quantification of myelin component,[9–12] by myelin water imaging (MWI). One method relies on the analysis of transversal relaxation times (T_2), because of its multi-component nature. Indeed, the T_2 of white matter has been established by several studies most of which agree on the decomposition of the decay signal into 3 main components, attributing to each component a different T_2: water trapped in the lipid bilayer membrane of myelin (T_2 around 10-20 ms), intra/extracellular water of the axonal cell (T_2 around 60-100 ms), and cerebrospinal fluid.[13]

It has been previously demonstrated that MRI by DTI and its related metrics provide an insight in the alterations induced by radiotherapy. Radial diffusivity (RD), axial diffusivity

(AD), and fractional anisotropy (FA) were previously investigated to detect radiation-associated changes in the axonal tissue.[7,14–24] In general, FA has been regarded as an indirect measure of myelination, even though the contribution of myelin to FA was shown to be limited.[9] Increased RD and decreased AD are expected to correspond to demyelination and axonal degeneration/gliosis, respectively.[7]

However, interpreting DTI as a sole myelin biomarker may lead to an incorrect interpretation of the result and MWI might provide additional information with respect to DTI.

In a prospective observational study that enrolled patients who received proton irradiation to the CNS, we investigated for the first time the potential of MWI by multi-component T_2 relaxometry as a quantitative imaging biomarker for radiation-induced image changes on CNS tissue, comparing them with those detected by a DTI technique.

2 | METHODS

2.1 | MR acquisitions

Patients were enrolled in a prospective, observational, institutional review board-approved study. Written informed consent was obtained for all participants. Images were acquired with a 1.5T MR scanner (Philips Ingenia system, Philips Medical Systems, Best, The Netherlands). The imaging protocol included an MWI and a DTI sequence. MWI was obtained using a multi-component T_2 relaxation technique by a 3D gradient and spin echo (GraSE) multi-echo sequence with the following parameters: TR = 1000 ms, 32 equally spaced echoes ranging from 10 to 320 ms, EPI factor = 5, FOV = 210 × 184 mm^2, acquisition matrix = 128 × 126 reconstructed to 256 × 256, 18 slices 5 mm thickness reconstructed to 36 slices 2.5 mm thickness. DTI was acquired by a multi-slice and multi-shot sequence (2 segments) with the following parameters TR = 2246 ms, TE = 85.5 ms, FOV = 256 × 256 mm^2, acquisition matrix = 128 × 102 reconstructed to 256 × 256, 18 slices 5 mm thickness, 15 directions with b = 1000 s/mm^2 and 1 b0 image. A second DTI sequence was acquired, equal to the previous one except for the phase encoding direction, which was reverted, to correct susceptibility distortions.[25] The total imaging time was ~9 min for MWI plus ~3 min for DTI. Both MWI and DTI scans were acquired before (*pre*) and immediately at the end (*end*) of the proton treatment.

Finally, a standard 3D T_1-weighted sequence was acquired before the radiation treatment, and standard 3D FLAIR images were acquired at *pre* and *end* PT for each patient.

2.2 | MR image processing

Multi-echo images were processed on a dedicated workstation by FSL, created by the Analysis Group (FMRIB, Oxford, UK),[26] MATLAB (The MathWorks, Natick, MA), and MERA.[27] The last is a free tool for multi-exponential relaxation analysis, which fits data with a distribution of decaying exponential functions. The analysis included fitting the refocusing flip angle[28] as implemented in MERA. Each volume of the multi-echo MWI data was smoothed by a 3D Gaussian kernel (SD = 1.5). Multi-echo data were then processed by MERA to identify in each voxel[29] 3 T_2 compartments from the obtained T_2 spectrum. The T_2 component below 40 ms was labeled as myelin water (Mw)[13] and indicated by Mw in the following, between 40 and 250 ms was labeled as intra-extracellular water (IEw in the following) and above 250 ms was considered as cerebrospinal fluid / free water (CSFw). The 40-250 ms range of the second component has been chosen to exclude the Mw component, but possibly to include tissue alterations,[30] hence, avoiding the exclusion of potentially informative regions. According to this labeling, three 3D maps were extracted describing the relative amplitude of the signal intensity in each compartment, that is, Mw is the area under the curve of the normalized T_2 spectrum ranging between 0 and 40 ms, IEw is the area between 40 and 250 ms, and CSFw is the area above 250 ms. The mean T_2 values of Mw and IEw components were also evaluated and 2 additional 3D maps were extracted. The mean T_2 time for the free water/CSF compartment is not reported, given that the longest measured echo time is only 320 ms and the estimate would not be accurate. A pictorial representation of the MWI image processing pipeline is shown in Figure 1.

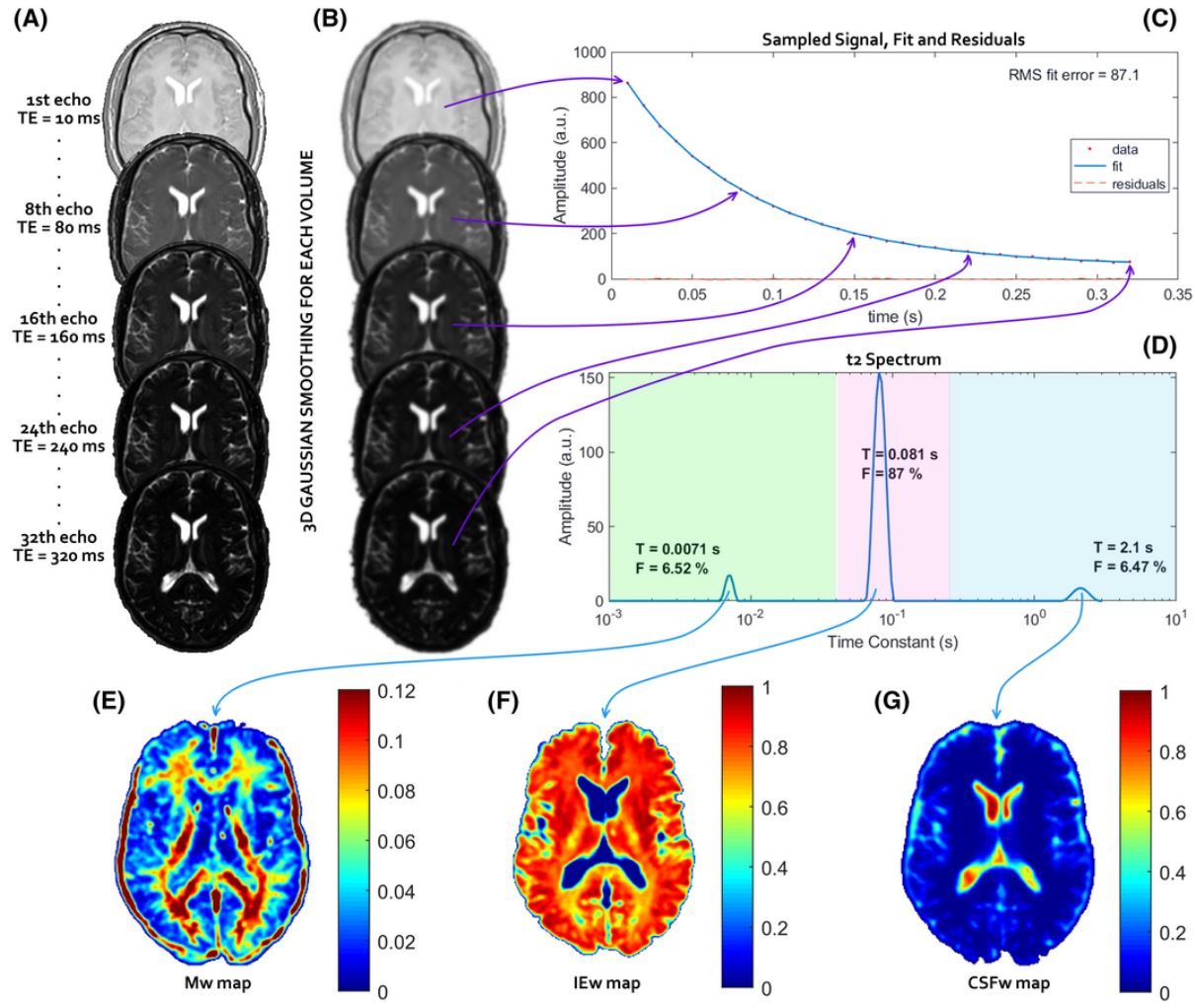

FIGURE 1. Myelin water imaging (MWI) image processing pipeline. Images acquired at 5 of the 32 echoes with the multi-echo gradient and spin echo (GraSE) sequence (A) and their corresponding Gaussian smoothed images (B). In each voxel, the decay signal (C) is fitted with a distribution of decaying exponential functions to extract the corresponding T_2-spectrum (D). In each voxel, the T_2 components below 40 ms are labeled as myelin water (Mw), between 40 and 250 ms as intra-extracellular water (IEw) and above 250 ms as cerebrospinal fluid/free water (CSFw) to obtain the corresponding Mw (E), IEw (F), and CSFw (G) maps

Diffusion images were corrected by FSL tools for B0 inhomogeneity[25] and for eddy currents distortion and patient movements.[31] Corrected images were then fitted by FSL with a diffusion tensor model[26] and the FA, AD, and RD maps were calculated.

2.3 | Data analysis

For each patient, the dose distribution was computed by the treatment planning system (RayStation, RaySearch Laboratories, Stockholm, Sweden). The gross target volume (GTV) and surgical cavity were manually contoured by expert radiation oncologists. A T_1-weighted sequence, acquired before the radiation treatment, was used as the reference for linear registration of all the generated MWI and DTI maps. Linear registration was performed by means of FSL tools.[32] In the same T_1-weighted

images, white matter, gray matter, and CSF were automatically segmented by FSL tools.[26]

In each patient, the dose distribution was corrected to account for the different fractionation. A biological equivalent dose (BED) was calculated in each voxel according to the following formula:

AQ7

$$\mathrm{BED} = n * d * \left(1 + \frac{d}{\alpha/\beta}\right), \quad (1)$$

where n is the number of fractions, d is the voxel dose per fraction, and α/β is an empirical parameter set equal to 2, in agreement with commonly accepted value for the central nervous system.

The registered BED, MWI, and DTI maps were analyzed in MATLAB. Voxel-wise difference maps were obtained by subtracting MWI and DTI *pre* maps from those acquired at *end* PT. An example of T_1, FA, AD, RD, and BED maps is shown in Supporting Information Figure S1.

For the analysis, to avoid inclusion of spurious/undesired data, only the voxels selected according to the following criteria were considered:

- Inclusion criteria:
  - Belonging to white-matter regions (based on T_1 segmentation)
  - BED > 0.01 Gy
  - Mw > 0 (for MWI data only)
  - FA > 0.3 (for DTI data only)
- Exclusion criteria:
  - GTV
  - Surgical cavity
  - Edema (based on the eventual signal hyper-intensity, which was manually outlined on FLAIR images acquired before or at the end of the proton treatment)

All the computed difference values of the voxels selected with the above criteria in all patients were then collected together in a unique difference data set. That data set was then sorted according to increasing voxel BED and grouped in 20 bins, both equally spaced and equally sized. For each bin, the mean percentage difference with respect to the baseline value, that is, equal to 100*(*end*–*pre*)/*pre*, was calculated and plotted against the corresponding mean BED value. The resulting data were finally fitted by a linear model with a weighted least square method. The weight of each bin was chosen

proportionally to the SEM of the same bin. A *P*-value lower than 0.05 was considered significant.

To evaluate the reproducibility of MWI measurements, a healthy volunteer was scanned twice in a week. The selection criteria included voxels belonging to white matter and Mw > 0.

3 | RESULTS

AQ8 A total of 16 patients were enrolled in the study. All the patients underwent fractionated proton therapy (PT) ~~and received~~receiving dose to the healthy CNS due to direct (brain tumors) or indirect (base skull tumors) irradiation. Patients' characteristics are listed in Table 1.

AQ9 **TABLE 1.** Patient characteristics

Patient No.	Age (y)/gender	Diagnosis	Location	Prescribe
1	34/M	Grade IV diffuse glioma	Brainstem	54/30
2	63/M	Chordoma	Skull base	74/37
3	68/M	Chordoma	Skull base	72/36
4	66/F	Chordoma	Skull base	74/37
5	54/M	Grade IV glioma	Right temporoparietal	36/18
6	65/M	Grade II glioma	Right frontal	59.4/33
7	84/F	Chordoma	Skull base	72/36
8	54/F	Grade II astrocytoma	Left frontal	54/27
9	20/F	Grade I astrocytoma	Cerebellum	54/27
10	22/F	High grade Pineoblastoma	Pineal region	54/30
11	26/M	Germinoma	Cerebellum/ventricles	40/25
12	59/M	Diffuse Glioma	Brainstem	54/30
13	54/F	Grade III astrocytoma	Right temporal	60/30
14	41/M	Grade III oligodendroglioma	Right frontal	59.4/33
15	20/M	Germinoma	Ventricles	54.4/34
16	69/F	Medulloblastoma	Cerebellum	54/30

Abbreviations: RBE, relative biological effectiveness.~~CTV, clinical target volume; GTV, gross tumor volume.~~
~~** If~~ AQ10 ~~16 patients, MWI and DTI were acquired both at *pre* and *end* PT.~~

A depiction of the voxel selection procedure for MWI data is exemplarily shown in Figure 2, on a slice of patient 6. Only white matter voxels were selected, excluding edema. Besides that, only the voxels where Mw > 0 at both time points were selected. This last restriction avoids including in the difference analysis voxels that were wrongly assigned with Mw = 0 because of noise in the MWI processing. The DTI threshold for voxel selection (FA > 0.3, not shown in Figure 2) was chosen because it is a typical value to discriminate between grey and white-matter.

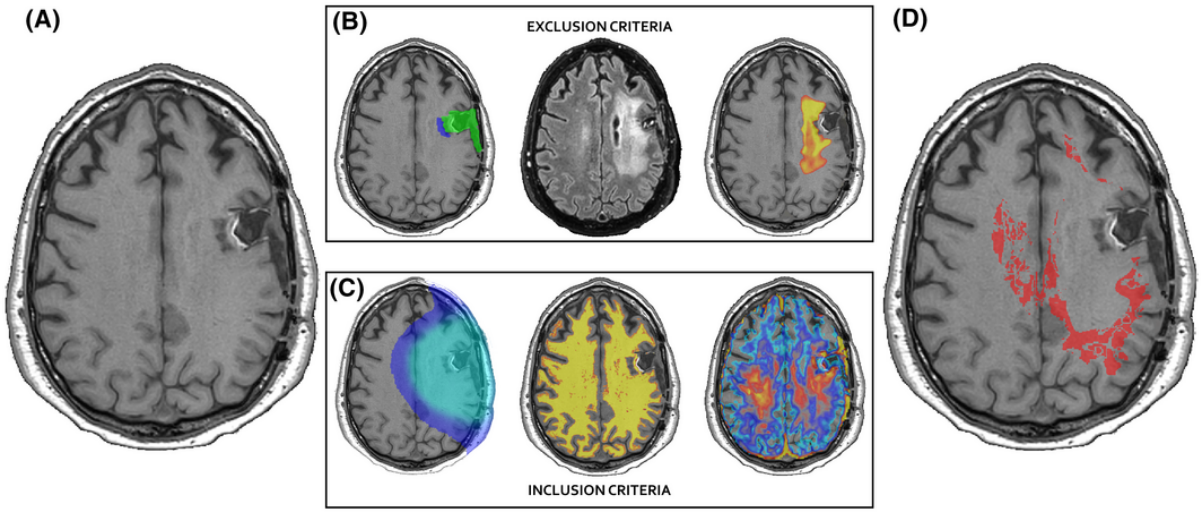

FIGURE 2. Myelin water imaging (MWI) voxel selection procedure. (A) T_1 image. (B) Exclusion areas: gross tumor volume (GTV) and surgical cavity (blue and green, respectively), were identified on the T_1 image (left), edema was identified on fluid-attenuated inversion recovery (FLAIR) image (middle) and then, the contoured region was copied on the co-registered T_1 image (right). (C) Inclusion areas: dose map was co-registered on the T_1 image (left), White matter was segmented on the T_1 image (middle) and myelin water (Mw) map was co-registered on the T_1 image (right). (D) Final voxel selection (red pixels) is shown on the T_1 image

A correlation analysis was performed between the delivered dose and the multi-echo derived maps differences, as reported in Figure 3, where Mw, IEw, and CSFw changes were correlated with the BED. All the voxels, selected with the above criteria, in all the patients, were collected together in a unique difference-data set. The analysis was performed both by equally sized bins (Figure 3 left), where the same number of voxels are considered in each bin, and by equally spaced bins (Figure 3 right), where, instead, the interval among bins was kept constant. In both analysis, the Mw percentage difference showed a positive correlation with BED ($P < .01$) and the IEw percentage difference showed a negative correlation with BED ($P < .01$). In contrast, the changes in the third component, identified as CSFw, did not reveal any significant correlation with

the delivered BED, as shown in Figure 3. The data of the healthy volunteer are reported in the plots as a red marker.

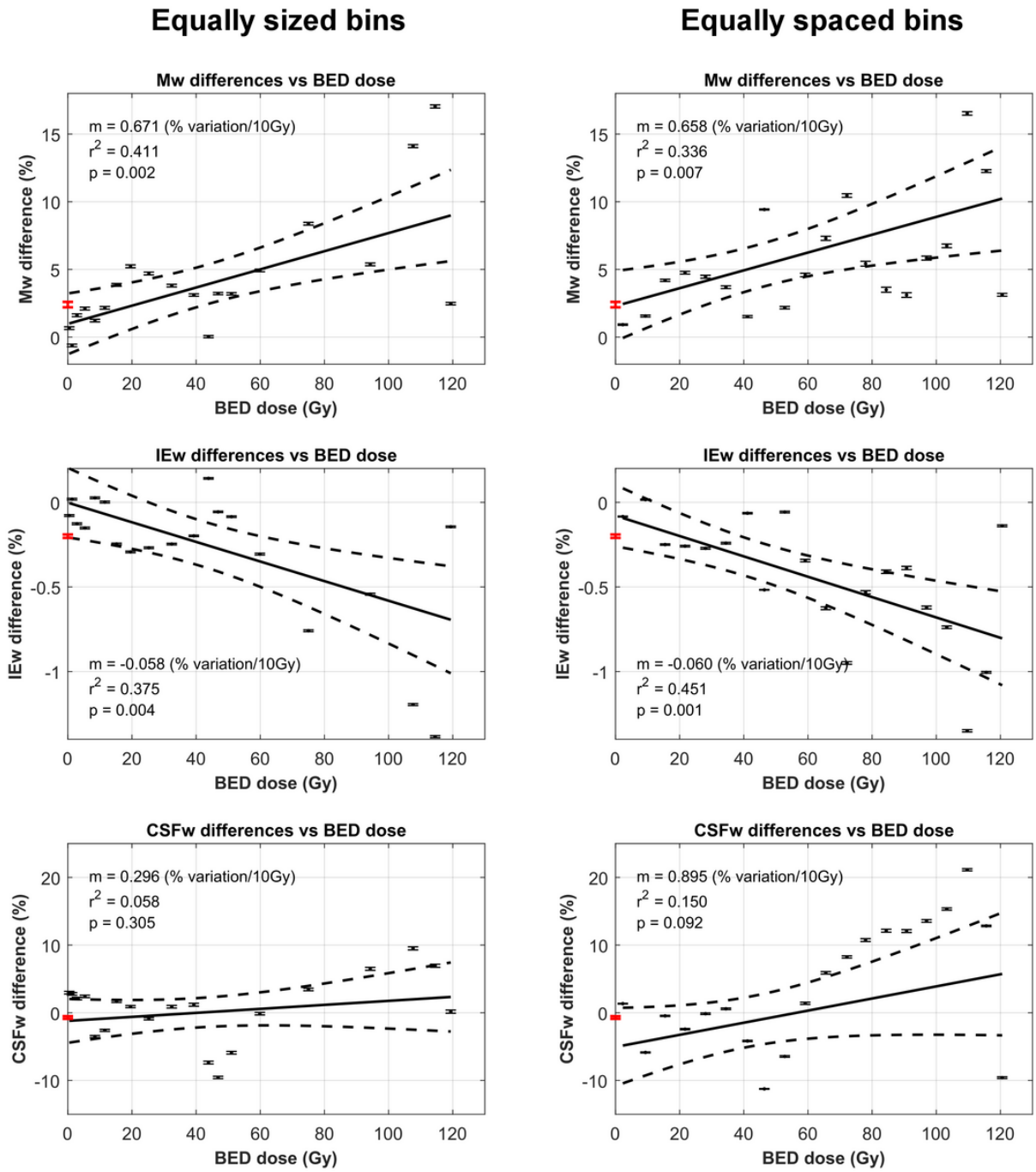

FIGURE 3. Myelin water imaging (MWI) versus biological equivalent dose (BED). Correlation analysis between the delivered dose and the difference maps obtained by equally sized bins (left) and equally spaced bins (right) analysis. Myelin water (Mw), intra-extracellular water (IEw), and cerebrospinal fluid/free water (CSFw) are shown from top to bottom. Data are reported as percentage variation with respect to baseline values. Error bars represent the SEM. The R^2 values and the corresponding *P*-values are reported on each panel. A *P*-value < .01 was considered significant. The dashed lines represent the 95% confidence interval of the linear fit (solid line). The data corresponding to the healthy volunteer are reported in the plots as a red marker

The analysis of mean T_2 values for both Mw and IEw components is reported in Supporting Information Figure S2, where no statistically significant correlation with BED was found.

The analysis of DTI maps, reported in Figure 4, revealed a significant (at a 0.01 level) positive correlation between FA changes and the delivered BED. The negative correlation between RD changes and the delivered BED was significant ($P < .05$) in the analysis by equally sized bins, but not significant ($P = .09$) in the analysis by equally spaced bins. The analysis of AD changes did not show a significant correlation with BED.

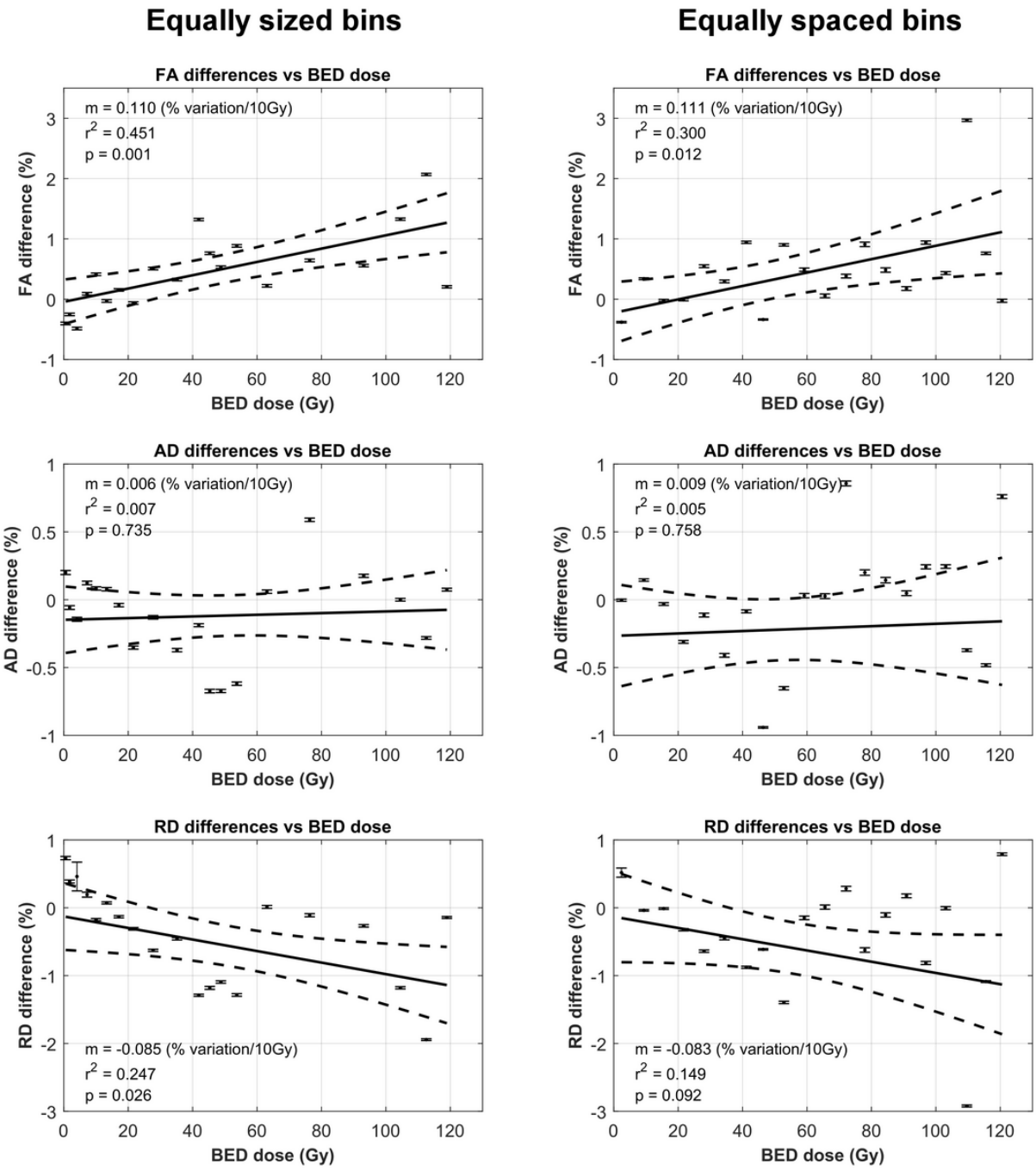

FIGURE 4. DTI versus biological equivalent dose (BED). Correlation analysis between the delivered dose and the difference maps obtained by equally sized bins (left) and equally spaced bins (right) analysis. Fractional anisotropy (FA), axial diffusivity (AD), and radial diffusivity (RD) are shown from top to bottom. Data are reported as percentage variation with respect to baseline values. Error bars represent the SEM. The R^2 values and the corresponding *P*-values are reported on each panel. A *P*-value < .01 was considered significant. The dashed lines represent the 95% confidence interval of the linear fit (solid line)

4 | DISCUSSION

Early pre-symptomatic detection of the post-radiation brain injury at the time when no conventional-MRI visible lesions have developed, besides increasing the knowledge on

the pathogenesis of the radiation damage, might be of great importance to identify radiosensitive tissue region and/or patients for early prevention and mitigation of complications.

Few studies investigated advanced MRI techniques to detect early white matter changes during or at the end of the radiation treatment, most of them by DTI as a biomarker. A decrease in AD and an increase in RD in specific brain structure during and after irradiation were observed.[14] When neurocognitive scores were investigated, DTI changes were predictive of neurocognitive decline.[7,14] In another study, the different white matter structures varied greatly in their response at the end of radiotherapy.[15] In all these structures, a significant increase of RD and a decrease of FA were observed both at the end and 1-month post radiotherapy, whereas AD reduction was significant only in fewer structures.[15] It was reported that DTI was not sensitive to acute global normal appearing white matter changes during the radiation treatment, but sensitive to early posttreatment changes, because the detected changes were significant at week 6 of the treatment, or immediately after radiotherapy.[33] These last data were somehow in agreement with our findings, as discussed below.

Early irradiation changes, in their pre-symptomatic phase, were also investigated by resting-state functional MRI measuring the BOLD signal,[34] showing an acute increase in local brain activity that was followed by extensive reductions in such activity and significant loss of functional connectivity. The vascular alteration was also investigated as a surrogate biomarker of radiation-induced injury by DCE MRI. Early assessment, from pre-irradiation to 1 month post-irradiation, of cerebral microvessel injury was detected by DCE-MRI parameters and was predictive of late neurocognitive dysfunction.[35,36] Finally, early assessment of perfusion by MRI arterial spin labeling during the course of radio-chemotherapy showed significant changes, which were higher in regions receiving a higher dose of radiation.[37]

Our study aims to investigate an MWI technique based on multicomponent T_2 relaxation, capable of characterizing water trapped in between lipid bilayer membrane of myelin and intra/extracellular water of the axonal cell, to detect early radiation-induced changes. Both the acquisition sequence and the data processing applied in this study were previously investigated by our group.[38] Our results suggest that MWI might be capable of detecting white matter alteration very early. In fact, both Mw and IEw showed clear significant changes comparing *end* treatment acquisition with respect to *pre*-treatment data. On the DTI data acquired at *end* treatment, only FA showed fully significant changes and the weaker significance of RD changes with respect to *pre*-treatment also depended on the chosen bin intervals. However, the quality of DTI images could have been improved using longer sequences. We preferred to rely on faster DTI sequences, limiting the total acquisition time for better compliance of the patient. At the same time, MWI is not a widely used method, and, differently from DTI, it cannot be considered a fully mature technique. There is room for improving the

sequence and method we applied, both in the acquisition phase and in the post-processing, to eventually improve image quality.

Our findings need to be confirmed on a larger cohort of patients and need a deeper investigation, including pre-clinical studies on experimental models, to be properly understood. The observed increase, proportionally to the dose, of Mw is suggestive of swelling of the myelin sheath. Cell swelling is known to be an early change that occurs in most types of acute cell injury, preluding to more drastic changes or simply disappearing as the cell adapts and repairs damage. The increase of Mw corresponded to an equal decrease, proportionally to the dose, of IEw, which might be because of
AQ11 intracellular shrinkage and/or reduction of the extracellular space. Despite the absolute changes in the Mw component were almost exactly compensated by the corresponding absolute changes in IEw, as an effect of the normalization applied to the T_2 spectrum, the relative percentage of variation of Mw was much greater than the percentage of variation of IEw, because Mw is much smaller than IEw. These changes might be compatible with the trends we observed on the corresponding DTI data, despite that the last were not fully significant. In fact, a decrease of RD might be suggestive of slight axonal shrinkage, with water translocation from the axial cylinder to the Schwann cell, where it does not contribute to the DTI signal because of short T_2 relaxation. An RD decrease might also produce a corresponding increase in FA. These results were unexpected, because the changes typically observed by DTI at follow-up after radiation therapy were, conversely, a decrease of FA and an increase of RD. However, as reported above, DTI early changes induced by the radiation insult are less certain and still poorly investigated and some transitory effects cannot be excluded a priori.

Our study had a limited scope, and therefore, it was affected by some limitations. In particular, we did not perform any analysis to take into account the different responses of white matter structures, which was evidenced by previous DTI studies.[19,20] All the selected voxels in all the patients were collected together in a unique difference-data set. In a future study on a larger cohort of patients, the different structure radio-
AQ12 sensitivity might be taken into account. Besides that, the subject population was very heterogeneous, including a mixture of different lesions, which behavior and response
AQ13 to radiotherapy are diverse. Nevertheless, our focus was exclusively on healthy brain tissue, being the lesions excluded from the analysis, so that the impact of different patient ~~groups~~lesions has been minimized.

Another limitation was the potential variable radiobiological effect of proton irradiation. PT is a radiation treatment alternative to conventional photon therapy, which is increasingly popular because of its physical characteristics allowing a lower entry/exit dose compared to photon irradiation. Because of the decrease in the dose to normal tissues it is expected to decrease treatment-related side effects and, compared to modern photon-based therapies, to reduce the risk of secondary neoplasms. The effectiveness of proton particles versus photons, regarding their potential to induce biological effects in the cells, is weighted with the relative biological effectiveness ,

which is typically assumed to be 1.1. However, the actual relative biological effectiveness may be higher and it may vary depending on the position along the proton depth dose curve. In our study, a variable relative biological effectiveness was not taken into account because it was not expected to affect the comparison between MWI and DTI and it was presumably too small to be easily detectable on the limited number of patients we investigated. At the same time, the sensitivity observed between MWI and DTI changes and BED promotes their application on a larger cohort of patients to also investigate variable relative biological effectiveness.

In conclusion, in our study MWI by T_2 relaxometry detected early white matter radiation-induced alterations, which might provide additional information with respect to those detected by DTI, that could improve the understanding of the pathogenesis of the radiation damage and deserves to be further investigated in the future in clinical studies on patients and in pre-clinical studies on experimental models.

ACKNOWLEDGMENT

Pietro Bontempi was supported by a grant founded by the Fondazione CARITRO, via Calepina 1, 38122 Trento, Italy.

Supporting Information

FIGURE S1 Representative T_1, FA, AD, RD, and BED maps of a study subject. Top: from left to right, T1, FA, AD, and RD images are shown with BED map as semi-transparent overlay. Bottom: same as top row without the overlay of BED map

FIGURE S2 Correlation analysis between the delivered dose and the difference maps obtained by equally sized bins (top) and equally spaced bins (bottom) analysis. Mean T_2 of Mw and IEw are shown from left to right. Data are reported as percentage variation with respect to baseline values. Error bars represent the SEM. The R^2 values and the corresponding *P*-values are reported on each panel. A *P*-value < .01 was considered significant. The dashed lines represent the 95% confidence interval of the linear fit (solid line)

REFERENCES

1 Sheline GE, Wara WM, Smith V. Therapeutic irradiation and brain injury. *Int J Radiat Oncol Biol Phys*. 1980;6 :1215-1228.

2 Wong CS, Van der Kogel AJ. Mechanisms of radiation injury to the central nervous system: implications for neuroprotection. *Mol Interventions*. 2004;4 :273-284.

3 Soussain C, Ricard D, Fike JR, Mazeron JJ, Psimaras D, Delattre JY. CNS complications of radiotherapy and chemotherapy. *Lancet*. 2009;374 :1639-1651.

4 Bentzen SM. Preventing or reducing late side effects of radiation therapy: radiobiology meets molecular pathology. *Nat Rev Cancer*. 2006;6 :702-713.

5 Tofilon PJ, Fike JR. The radioresponse of the central nervous system: a dynamic process. *Radiat Res*. 2000;153 :357-370.

6 Freeman JE, Johnston PG, Voke JM. Somnolence after prophylactic cranial irradiation in children with acute lymphoblastic leukaemia. *Br Med J*. 1973;4 :523-525.

7 Chapman CH, Zhu T, Nazem-Zadeh M, et al. Diffusion tensor imaging predicts cognitive function change following partial brain radiotherapy for low-grade and benign tumors. *Radiother Oncol*. 2016;120 :234-240.

8 Schultheiss TE, Stephens LC, Maor MH. Analysis of the histopathology of radiation myelopathy. *Int J Radiat Oncol Biol Phys*. 1988;27 :27-32.

AQ14 9 Lee J, Hyun J-W, Lee J, et al. So you want to image myelin using MRI: an overview and practical guide for myelin water imaging. *J Magn Reson Imaging*. ~~2020~~2021.53 (2):360–373.

10 Heath F, Hurley SA, Johansen-Berg H, Sampaio-Baptista C. Advances in noninvasive myelin imaging. *Dev Neurobiol*. 2018;78 :136-151.

11 Laule C, Vavasour IM, Kolind SH, et al. Magnetic resonance imaging of myelin. *Neurotherapeutics*. 2007;4 :460-484. Review.

12 Alonso-Ortiz E, Levesque IR, Pike GB. MRI-based myelin water imaging: a technical review. *Magn Reson Med*. 2015;73 :70-81.

13 MacKay AL, Laule C. Magnetic resonance of myelin water: an in vivo marker for myelin. *Brain Plast*. 2016;2 :71-91.

14 Chapman CH, Nagesh V, Sundgren PC, et al. Diffusion tensor imaging of normal-appearing white matter as biomarker for radiation-induced late delayed cognitive decline. *Int J Radiat Oncol Biol Phys*. 2012;82 :2033-2040.

15 Chapman CH, Nazem-Zadeh M, Lee OE, et al. Regional variation in brain white matter diffusion index changes following chemoradiotherapy: a prospective study using tract-based spatial statistics. *PLoS One*. 2013;8 :e57768.

16 Connor M, Karunamuni R, McDonald C, et al. Dose-dependent white matter damage after brain radiotherapy. *Radiother Oncol*. 2016;121 :209-216.

17 Karunamuni RA, White NS, McDonald CR, et al. Multi-component diffusion characterization of radiation-induced white matter damage. *Med Phys*. 2017;44 :1747-1754.

18 Raschke F, Wesemann T, Wahl H, et al. Reduced diffusion in normal appearing white matter of glioma patients following radio(chemo)therapy. *Radiother Oncol*. 2019;140 :110-115.

19 Zhu T, Chapman CH, Tsien C, et al. Effect of the maximum dose on white matter fiber bundles using longitudinal diffusion tensor imaging. *Int J Radiat Oncol Biol Phys*. 2016;96 :696-705.

20 Connor M, Karunamuni R, McDonald C, et al. Regional susceptibility to dose-dependent white matter damage after brain radiotherapy. *Radiother Oncol*. 2017;123 :209-217.

21 Uh J, Merchant TE, Li Y, et al. Differences in brainstem fiber tract response to radiation: a longitudinal diffusion tensor imaging study. *Int J Radiat Oncol Biol Phys*. 2013;86 :292-297.

22 Hua C, Merchant TE, Gajjar A, et al. Brain tumor therapy-induced changes in normal-appearing brainstem measured with longitudinal diffusion tensor imaging. *Int J Radiat Oncol Biol Phys*. 2012;82 :2047-2054.

23 Leung LH, Ooi GC, Kwong DL, Chan GC, Cao G, Khong PL. White-matter diffusion anisotropy after chemo-irradiation: a statistical parametric mapping study and histogram analysis. *Neuroimage*. 2004;21 :261-268.

24 Qiu D, Leung LH, Kwong DL, Chan GC, Khong PL. Mapping radiation dose distribution on the fractional anisotropy map: applications in the assessment of treatment-induced white matter injury. *Neuroimage*. 2006;31 :109-115.

25 Andersson JL, Skare S, Ashburner J. How to correct susceptibility distortions in spin-echo echo-planar images: application to diffusion tensor imaging. *Neuroimage*. 2003;20 :870-888.

26 Smith SM, Jenkinson M, Woolrich MW, et al. Advances in functional and structural MR image analysis and implementation as FSL. *Neuroimage*. 2004;23 :S208-S219.

27 MERA. *Multi Exponential Relaxation Analysis toolbox for MATLAB*. Free download available at https://github.com/markdoes/MERA.

28 Prasloski T, Mädler B, Xiang QS, MacKay A, Jones C. Applications of stimulated echo correction to multicomponent T2 analysis. *Magn Reson Med*. 2012;67 :1803-1814.

29 Meyers SM, Laule C, Vavasour IM, et al. Reproducibility of myelin water fraction analysis: a comparison of region of interest and voxel-based analysis methods. *Magn Reson Imaging*. 2009;27 :1096-1103.

30 Stewart WA, MacKay AL, Whittall KP, Moore GR, Paty DW. Spin-spin relaxation in experimental allergic encephalomyelitis. Analysis of CPMG data using a non-linear least squares method and linear inverse theory. *Magn Reson Med*. 1993;29 :767-775.

31 Andersson JLR, Sotiropoulos SN. An integrated approach to correction for off-resonance effects and subject movement in diffusion MR imaging. *Neuroimage*. 2016;15 :1063-1078.

32 Jenkinson M, Bannister P, Brady M, Smith S. Improved optimization for the robust and accurate linear registration and motion correction of brain images. *Neuroimage*. 2002;17 :825-841.

33 Hope TR, Vardal J, Bjørnerud A, et al. Serial diffusion tensor imaging for early detection of radiation-induced injuries to normal-appearing white matter in high-grade glioma patients. *J Magn Reson Imaging*. 2015;41 :414-423.

34 Ding Z, Zhang H, Lv X-F, et al. Radiation-induced brain structural and functional abnormalities in presymptomatic phase and outcome prediction. *Hum Brain Mapp*. 2018;39 :407-427.

35 Cao Y, Tsien CI, Sundgren PC, et al. Dynamic contrast-enhanced magnetic resonance imaging as a biomarker for prediction of radiation-induced neurocognitive dysfunction. *Clin Cancer Res*. 2009;15 :1747-1754.

36 Farjam R, Pramanik P, Aryal MP, et al. A radiation-induced hippocampal vascular injury surrogate marker predicts late neurocognitive dysfunction. *Int J Radiat Oncol Biol Phys*. 2015;93 :908-915.

37 Petr J, Platzek I, Seidlitz A, et al. Early and late effects of radiochemotherapy on cerebral blood flow in glioblastoma patients measured with non-invasive perfusion MRI. *Radiother Oncol*. 2016;118 :24-28.

38 Bontempi P, Rozzanigo U, Amelio D, Scartoni D, Amichetti M, Farace P. Quantitative multicomponent T2 relaxation showed greater sensitivity than flair imaging to detect subtle alterations at the periphery of lower grade gliomas. *Front Oncol*. 2021;22 :651137.

How to cite this article: Bontempi P, Scartoni D, Amelio D, et al. Multicomponent T_2 relaxometry reveals early myelin white matter changes induced by proton radiation treatment. *Magn Reson Med*. 2021;00 :000–000. https://doi.org/10.1002/mrm.28913

---------- End of Document ----------